

# Identification of boundary heat fluxes in a falling film experiment using high resolution temperature measurements

Sven Groß<sup>a</sup>, Marcus Soemers<sup>a</sup>, Adel Mhamdi<sup>b</sup>, Faruk Al Sibai<sup>c</sup>  
Arnold Reusken<sup>a</sup>, Wolfgang Marquardt<sup>b,\*</sup>, Ulrich Renz<sup>c</sup>

<sup>a</sup> *Chair of Numerical Mathematics, RWTH Aachen University*

<sup>b</sup> *Chair of Process Systems Engineering, RWTH Aachen University*

<sup>c</sup> *Chair of Heat Transfer and Air Conditioning, RWTH Aachen University*

---

## Abstract

In this paper, we consider a three-dimensional inverse heat conduction problem (IHCP) in a falling film experiment. The wavy film is heated electrically by a thin constantan foil and the temperature on the back side of this foil is measured by high resolution infrared (IR) thermography. The transient heat flux at the inaccessible film side of the foil is determined from the IR data and the electrical heating power. The IHCP is formulated as a mathematical optimization problem, which is solved with the conjugate gradient method. In each step of the iterative process two direct transient heat conduction problems must be solved. We apply a one step  $\theta$ -method and piecewise linear finite elements on a tetrahedral grid for the time and space discretization, respectively. The resulting large sparse system of equations is solved with a preconditioned Krylov subspace method. We give results of simulated experiments, which illustrate the performance and tuning of the solution method, and finally present the estimation results from temperature measurements obtained during falling film experiments.

*Key words:* Inverse problem, regularization, conjugate gradient method, falling film, heat flux estimation, anisotropic finite elements, model-based experimental analysis

---

---

\* Corresponding author: Tel.: +49-241-8096712 ; Fax: +49-241-8092326; email: marquardt@lpt.rwth-aachen.de

# 1 Introduction

The modeling of kinetic phenomena in multiphase systems leads to problems of model structure and parameter identification, which belong to the class of inverse problems [14]. A challenging problem relates to the transport mechanisms in inverse heat and mass transfer problems.

In this paper, we focus on the heat transfer into a falling film. Fig. 1 shows the schematic representation of the falling film experiment operated in our research. It consists of the fluid cycle with a loudspeaker to produce 2D-waves

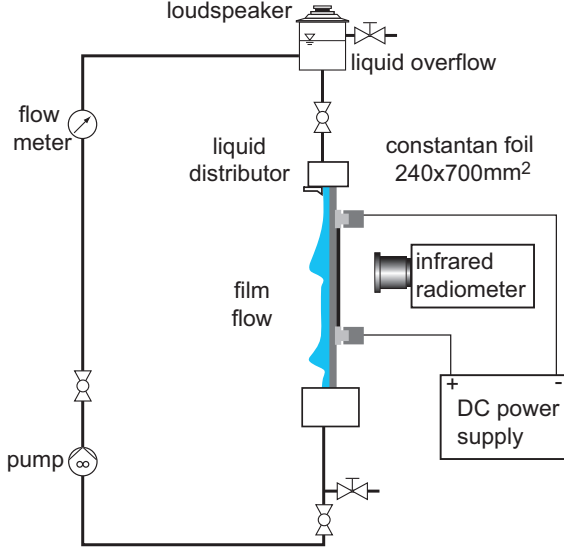


Fig. 1. Schematic representation of the falling film experiment

with a certain frequency, the laminar wavy falling film travelling along one side of a thin heating foil (with electrical heating via the DC power supply) and the infrared camera for taking temperature measurements on the foil back side with high resolution in space and time [1,12]. There are two alternatives for modeling the electrical heating at the back side of the thin constantan foil. We could consider a volumetric source term in the heat conduction equations or alternatively – as done in this paper – we can assume that we have a constant boundary heat flux. We use the temperature measurements to estimate the heat flux on the film side of the foil as a function of space and time with the remaining initial and boundary conditions assumed to be known. This is a model-free estimation problem, since no further assumptions on the heat transfer mechanism are made. In subsequent steps the estimated heat flux can be correlated with other quantities in the falling film such as the mean film temperature and the flow regime to obtain a better understanding of the related kinetic phenomena. The goal is not only the solution of this particular inverse heat transfer problem, but also to gain a better understanding of solution methods for multidimensional non-linear inverse problems in multi-

phase flow systems. Such an understanding is essential as a basis for future investigations of more complex inverse transport problems such as heat transfer through the falling film, mass transfer from the film to the gas phase, or reaction inside the film.

The identification problem of estimating the heat flux on the film surface is coupled with the fluid dynamics of the falling film. This coupling results in an inverse problem of very high complexity. In this paper, we consider a simplified, but still challenging and interesting problem in which we decouple the heat transfer from the fluid dynamics. We investigate the unsteady heat transfer from the heating foil to the falling film. The considered inverse heat conduction problem consists of determining the heat flux  $q_c(\mathbf{x}, t)$  on the film side of the foil  $\Gamma_2$  from measurement data  $T_m$ , which are taken on the foil back side  $\Gamma_1$ . These measurements are clearly influenced by the transport phenomena in the falling film and by the surface wave pattern. Fig. 2 shows the schematic representation of the three-dimensional plate  $\Omega \subset \mathbb{R}^3$  with heat addition on  $\Gamma_1$  and heat transfer on  $\Gamma_2$ .

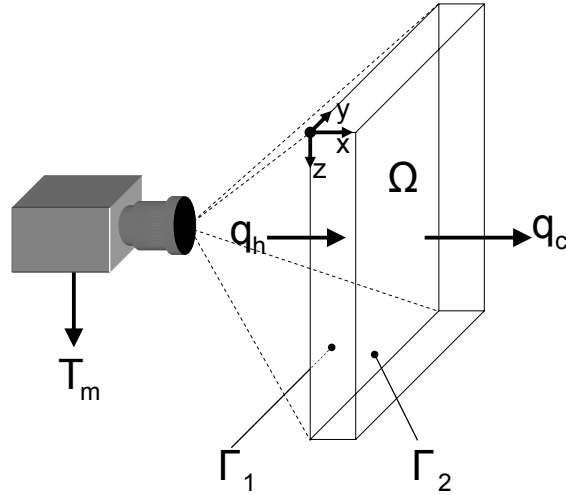


Fig. 2. Schematic representation of the 3D heating foil

Many studies related to IHCPs have already been published (cf. [2,5] and the references therein). Most literature on numerical solution methods is restricted to one or two space dimensions. For problems in three space dimensions only few publications are available [6,10,19]. In these papers only simulated data with few point-wise measurement locations have been used. Recently, an efficient method for the solution of transient 3D IHCPs has been published and applied to experimental investigations of pool boiling [13]. In contrast to this

filter-based method of limited space-time resolution, in this paper we investigate an optimization-based solution of the 3D IHCP for the reconstruction of boundary heat fluxes with high resolution in space and time employing high resolution spatio-temporal temperature measurements. Although the problem geometry is simple, there is a numerical complication caused by the plate thickness ( $25 \mu m$ ), which is very small compared to its other dimensions. Due to this geometric anisotropy one has to be careful in the choice of the solution methods for the direct problems.

The paper is organized as follows. The inverse problem is formulated as an optimization problem in Section 2. In Section 3 the solution method based on conjugate gradients (CG) is introduced. The solution methods for the direct problems that occur in the optimization procedure are discussed in Section 4. Some test examples for the validation of the IHCP solver are presented in Section 5, while results employing experimental measurement data are given in Section 6. Section 7 contains some conclusions and remarks concerning future work.

## 2 Formulation of the inverse problem

We consider the domain  $\Omega$  shown in Fig. 2 with boundary  $\partial\Omega = \Gamma_1 \cup \Gamma_2 \cup \Gamma_r$ , where  $\Gamma_1, \Gamma_2$  and  $\Gamma_r$  denote the measurement side, the film side and the remaining boundaries of the heating foil. The *direct problem* consists of the following heat conduction equation for the temperature  $T$

$$\frac{\partial T}{\partial t}(\mathbf{x}, t) = a \Delta T(\mathbf{x}, t), \quad (\mathbf{x}, t) \in \Omega \times [t_0, t_f], \quad (1)$$

$$T(\mathbf{x}, t_0) = T_0(\mathbf{x}), \quad \mathbf{x} \in \Omega, \quad (2)$$

$$-\lambda \frac{\partial T}{\partial n}(\mathbf{x}, t) = q_h(\mathbf{x}, t), \quad (\mathbf{x}, t) \in \Gamma_1 \cup \Gamma_r \times [t_0, t_f], \quad (3)$$

$$-\lambda \frac{\partial T}{\partial n}(\mathbf{x}, t) = q_c(\mathbf{x}, t), \quad (\mathbf{x}, t) \in \Gamma_2 \times [t_0, t_f], \quad (4)$$

where  $T_0, q_h$  and  $q_c$  are the initial and boundary conditions, respectively. The outer normal on the boundary is denoted by  $n$ . The initial and final times are denoted by  $t_0$  and  $t_f$ , respectively. The known material properties density  $\rho$ , specific heat  $c$  and heat conductivity  $\lambda$  enter the thermal diffusivity  $a = \frac{\lambda}{\rho c}$ , which is assumed to be constant, since the experimental temperature range is very small.

The *inverse problem* corresponds to the estimation of the heat flux  $q_c$  on  $\Gamma_2$  on the basis of suitable measurement data  $T_m$  on  $\Gamma_1$ , under the assumption

that the values of  $T_0$  and  $q_h$  are known. This is a typical example of an inverse heat conduction problem.

In this work we consider an optimization-based formulation, since it can easily be adapted to more complex situations. The unknown quantity  $q_c$  is determined in such a way that

$$J(\mathbf{x}, t; q_c) := \frac{1}{2} \|T(\mathbf{x}, t; q_c)|_{\Gamma_1} - T_m(\mathbf{x}, t)\|_{L_2}^2 \rightarrow \min \quad (5)$$

with  $T(\mathbf{x}, t; q_c)$  given by (1) – (4).

To emphasize the dependence of  $T$  on the boundary heat flux  $q_c$  we refer to the solution of (1)-(4) as  $T(\mathbf{x}, t; q_c)$ . The corresponding norm in (5) is defined by

$$\|\cdot\|_{L_2}^2 := \int_{t_0}^{t_f} \int_{\Gamma_1} (\cdot)^2 d\mathbf{x} dt. \quad (6)$$

Regularization [7] is only introduced via the discretization and suitable stopping criteria for the optimization algorithm. This strategy is discussed below in more detail. An alternative approach is to add a regularizing term  $R(q_c)$  to the objective function  $J$ , which penalizes the variation of  $q_c$ . This method will be considered in future work.

### 3 Minimization algorithm

For the solution of the least squares problem (5) many methods are available [2,3,7]. Here, we use the *conjugate gradient (CG) method* (see [7,16] for details), which is very efficient in terms of the number of iterations compared to other semi-iterative methods, if the discrepancy principle is chosen as a stopping rule [7]. For nonlinear problems, some variants of this algorithm are available in the literature [16].

The CG method solves the minimization problem by setting up an iteration sequence for the unknown function  $q_c$  (see Fig. 3). Here, the solution at iteration  $n$  is updated from the previous one until some stopping conditions are fulfilled. For the determination of the search direction the so-called conjugate gradients are used. So we have to calculate the gradient of the functional (5) to compute the search direction. The gradient is defined as the first order Fréchet derivative of the functional at some point  $q_c \in W$ , where  $W$  is a suitable function space. We consider the space  $W$  of continuous and piecewise linear functions on  $\Gamma_2$  which is due to the discretization of the domain  $\Omega$  with P1-elements on a tetrahedral grid. If the functional increment at some point

$q_c$  is given by

$$J(q_c + \delta q_c) - J(q_c) = \int_{t_0}^{t_f} \int_{\Gamma_2} \nabla J(\mathbf{x}, t) \delta q_c(\mathbf{x}, t) d\mathbf{x} dt + o(\|\delta q_c\|) \quad (7)$$

with  $q_c + \delta q_c \in W$ , then the function  $\nabla J(\mathbf{x}, t)$  is the *functional gradient* at  $q_c$ .

The CG procedure, illustrated in Fig. 3, comprises the following calculation steps:

- (i) Set  $n = 0$  and choose a starting value  $q_c^0 \in W$ , e.g.  $q_c^0 \equiv 0$ .
- (ii) Calculate the objective function. If the convergence conditions are satisfied stop, otherwise continue.
- (iii) Calculate the new search direction  $p^n = \nabla J(q_c^n) + \gamma^n p^{n-1}$ . The gradient  $\nabla J(q_c^n)$  is obtained from the solution of the *adjoint problem* (cf. Section 3.1). The *conjugate coefficient*  $\gamma^n$ ,  $n \geq 1$ , is determined from the expression

$$\gamma^n = - \frac{\int_{t_0}^{t_f} \int_{\Gamma_2} \nabla J(q_c^n) [\nabla J(q_c^{n-1}) - \nabla J(q_c^n)] d\mathbf{x} dt}{\int_{t_0}^{t_f} \int_{\Gamma_2} [\nabla J(q_c^{n-1})]^2 d\mathbf{x} dt} \quad (8)$$

and  $\gamma^0 = 0$ .

- (iv) Calculate the step length along the search direction by solving the one-dimensional optimization problem

$$\mu^n = \operatorname{argmin}_{\mu \geq 0} J(q_c^n - \mu p^n). \quad (9)$$

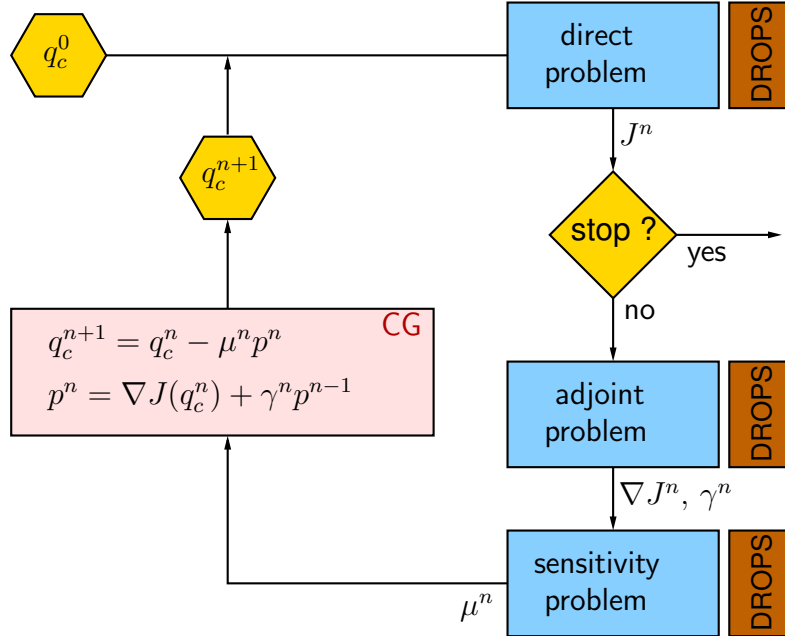


Fig. 3. CG method - iterative procedure

In our case  $\mu^n$  is given by

$$\mu^n = \frac{\int_{t_0}^{t_f} \int_{\Gamma_2} [T(\mathbf{x}, t; q_c^n) - T_m(\mathbf{x}, t)] S(\mathbf{x}, t) d\mathbf{x} dt}{\int_{t_0}^{t_f} \int_{\Gamma_2} [S(\mathbf{x}, t)]^2 d\mathbf{x} dt}, \quad (10)$$

with  $S$  being the solution of the *sensitivity problem* (cf. Section 3.2).

(v) Update the approximation

$$q_c^{n+1} = q_c^n - \mu^n p^n. \quad (11)$$

Increase  $n$  by one and go back to (ii).

Two difficulties arise in applying this solution approach. First we have to calculate the functional gradient and second we have to solve the optimization problem in (9) to find a step length along the descent direction. In the next section we discuss these two issues.

### 3.1 Adjoint problem

In the iterative gradient-based procedure, we need the gradient  $\nabla J(\mathbf{x}, t)$  to calculate the descent direction  $p^n$ . It can be shown that the identity

$$\nabla J(\mathbf{x}, t) = \psi(\mathbf{x}, t)|_{\Gamma_2} \quad (12)$$

holds, where the adjoint variable  $\psi$  is the solution of the *adjoint problem*

$$\frac{\partial \psi}{\partial t}(\mathbf{x}, t) = -a \Delta \psi(\mathbf{x}, t), \quad (\mathbf{x}, t) \in \Omega \times [t_0, t_f], \quad (13)$$

$$\psi(\mathbf{x}, t_f) = 0, \quad \mathbf{x} \in \Omega, \quad (14)$$

$$-\lambda \frac{\partial \psi}{\partial n}(\mathbf{x}, t) = [T(\mathbf{x}, t; q_c) - T_m(\mathbf{x}, t)], \quad (\mathbf{x}, t) \in \Gamma_1 \times [t_0, t_f], \quad (15)$$

$$-\lambda \frac{\partial \psi}{\partial n}(\mathbf{x}, t) = 0, \quad (\mathbf{x}, t) \in \Gamma_2 \cup \Gamma_r \times [t_0, t_f]. \quad (16)$$

We do not give a derivation of the identity in (12) since it follows from standard procedures [2]. For the adjoint problem we do not have an initial condition, but rather a condition at final time  $t_f$ . By introducing a new time variable  $t_b = t_f - t$ , we get an equation system which has the same structure as the original direct problem (1)-(4), however, with different initial and boundary conditions.

### 3.2 Sensitivity problem

The step length  $\mu^n$  along the search direction  $p^n$  is obtained from the solution of the *sensitivity problem* given by

$$\frac{\partial S}{\partial t}(\mathbf{x}, t) = a\Delta S(\mathbf{x}, t), \quad (\mathbf{x}, t) \in \Omega \times [t_0, t_f], \quad (17)$$

$$S(\mathbf{x}, t_0) = 0, \quad \mathbf{x} \in \Omega, \quad (18)$$

$$-\lambda \frac{\partial S}{\partial n}(\mathbf{x}, t) = 0, \quad (\mathbf{x}, t) \in \Gamma_1 \cup \Gamma_r \times [t_0, t_f], \quad (19)$$

$$-\lambda \frac{\partial S}{\partial n}(\mathbf{x}, t) = p^n(\mathbf{x}, t), \quad (\mathbf{x}, t) \in \Gamma_2 \times [t_0, t_f]. \quad (20)$$

Again, it has the same structure as the direct problem (1)-(4), but with different initial and boundary conditions.

In the iterative process, three direct heat conduction problems, the *direct*, *adjoint* and *sensitivity* problems, have to be solved. To calculate the corresponding solutions the same software code can be used, since all of the mentioned problems have the same structure. In many publications on the CG method, the three direct problems are solved at each iteration. Actually, in the particular case of linear problems only the solutions of *two* direct problems are needed in each optimization iteration (see Fig. 3) because of the identity

$$T(q_c^{n+1}) = T(q_c^n) - \mu^n S, \quad (21)$$

where  $S$  is the solution of the *sensitivity problem* (17)-(20). So the *direct problem* (1)-(4) is only solved once at the very beginning (i.e.  $n = 0$ ). This results in a substantial reduction of the computational time.

## 4 Solution of the direct problems

The solution of the direct 3D heat conduction equations is computed using the software package DROPS (cf. [8]), which is based on multilevel nested grids and finite element discretization methods. Some aspects of the numerical methods implemented in DROPS are briefly described in this section. For the time discretization, a standard one step  $\theta$ -method is used [15]. Piecewise linear finite elements on a tetrahedral grid are employed for the space discretization [17]. The resulting discrete systems of equations are solved with a preconditioned Krylov subspace method.

We outline the finite element method that is used for the *space discretization*. It is based on a variational formulation of the direct problem: For  $t \in [t_0, t_f]$



find  $T(t) \in V$  such that

$$\left(\frac{\partial T(t)}{\partial t}, v\right) + (a \nabla T(t), \nabla v) = -\frac{a}{\lambda} \int_{\partial\Omega} qv \, d\sigma \quad \forall v \in V. \quad (22)$$

Here  $V$  is a suitable function space (the Sobolev space  $H^1(\Omega)$ ) and  $(u, v) := \int_{\Omega} u \cdot v \, d\mathbf{x}$  denotes the  $L_2(\Omega)$  scalar product. For notational convenience we introduce the bilinear form  $\alpha(u, v) := (a \nabla u, \nabla v)$  and the functional  $\beta(t; v)$  which is defined by the right hand side in (22). The variational problem can be rewritten in compact form as

$$\left(\frac{\partial T(t)}{\partial t}, v\right) + \alpha(T(t), v) = \beta(t; v) \quad \forall v \in V.$$

For the discretization we use a triangulation  $\mathcal{T}$  of  $\Omega$  which consists of tetrahedra. The finite element space  $V_h \subset V$  consists of continuous piecewise linear functions. The degrees of freedom are located at the vertices of the tetrahedra. Let  $\{\varphi_i\}_{1 \leq i \leq N}$  be the standard nodal basis of the space  $V_h$ . The discrete problem is then given as follows: Find  $T_h \in V_h$  such that

$$\left(\frac{\partial T_h(t)}{\partial t}, \varphi_i\right) + \alpha(T_h(t), \varphi_i) = \beta(t; \varphi_i) \quad \forall 1 \leq i \leq N. \quad (23)$$

This is a system of coupled ordinary differential equations. For the *time discretization* a one step  $\theta$ -scheme is applied. The time step size is denoted by  $\tau$  and the approximate solution at time  $t_k$  is denoted by  $T_h^k$ . Then given  $T_h^k$ , we get the approximate solution  $T_h^{k+1} \approx T(t_{k+1}, \cdot)$  by solving the problem

$$\begin{aligned} (T_h^{k+1}, \varphi_i) + \theta \tau \alpha(T_h^{k+1}, \varphi_i) &= (T_h^k, \varphi_i) - (1 - \theta) \tau \alpha(T_h^k, \varphi_i) \\ &\quad + \theta \tau \beta(t_{k+1}; \varphi_i) + (1 - \theta) \tau \beta(t_k; \varphi_i), \end{aligned} \quad (24)$$

$$\forall 1 \leq i \leq N.$$

The parameter  $0 \leq \theta \leq 1$  controls the implicitness of the scheme. In particular,  $\theta = 0$  yields the explicit Euler scheme,  $\theta = 1$  the implicit Euler scheme and  $\theta = 0.5$  leads to the Crank-Nicholson scheme. Because of the strong stiffness of the system in (23) only implicit schemes ( $\theta \neq 0$ ) should be used to solve the instationary heat conduction problems. The implicit Euler scheme is only first order accurate (i.e. the discretization error is  $\mathcal{O}(\tau)$ ), but is strongly A-stable. The Crank-Nicholson scheme is of order two, is A-stable, but does not have the strong A-stability property, which may lead to stability problems in certain situations. In the remainder of this paper we only consider  $\theta = 0.5$  and  $\theta = 1$ .

Let  $\mathbf{u} \in \mathbb{R}^N$  be the coefficient vector of the representation of  $T_h = \sum_{i=1}^N u_i \varphi_i$  in the nodal basis. Equation (24) then represents a linear system of equations

for the unknown function  $T_h^{k+1}$ , which can be written as

$$[M + \theta\tau A] \mathbf{u}^{k+1} = [M - (1 - \theta)\tau A] \mathbf{u}^k + \theta\tau \mathbf{b}^{k+1} + (1 - \theta)\tau \mathbf{b}^k .$$

Here  $M$  denotes the mass matrix and  $A$  the stiffness matrix

$$M_{ij} := (\varphi_j, \varphi_i) , \quad A_{ij} := \alpha(\varphi_j, \varphi_i)$$

and  $\mathbf{b}^k, \mathbf{b}^{k+1}$  are the right hand sides with

$$\mathbf{b}_i^k = \beta(t_k; \varphi_i) , \quad \mathbf{b}_i^{k+1} = \beta(t_{k+1}; \varphi_i) .$$

The system matrix  $M + \theta\tau A$  is symmetric positive definite, thus a preconditioned conjugate gradient (PCG) method can be applied to solve this system of linear equations [18]. For the simulations presented in this paper we use the SSOR method for preconditioning.

At the end of this section, we briefly comment on the performance of the developed solver, because we consider a very thin heating foil. In this context we mention the properties of the applied triangulation technique and the arising degenerated tetrahedra (see Fig. 4 and 5). The standard kind of triangulation

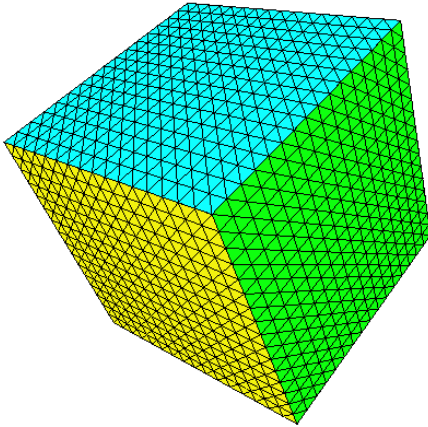


Fig. 4. Triangulation of the unit cube

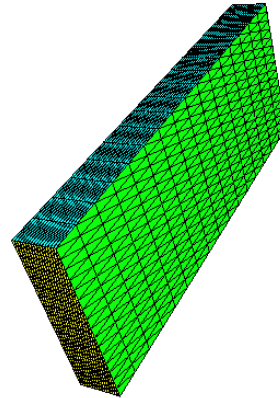


Fig. 5. Triangulation of a geometrical anisotropic domain

tion used within the software package DROPS avoids large angles inside the faces as well as between two faces of each tetrahedron, independent of the geometry dimension (for more information see [8]). Taking into consideration the so-called *maximum angle principle* (see [4,11]) we do not expect a loss of quality with respect to the discretizations of the involved direct heat conduction problems in the case of increasing anisotropy. This is confirmed by numerical experiments. However, we expect that the efficiency of the PCG

solver decreases with increasing geometrical degeneracy, which has been observed in numerical experiments, too. In this paper, we will not analyze these observations in more detail.

## 5 Simulation examples for method and code validation

The DROPS code as well as the optimization method were validated via various simulations. Some results of these case studies are given in this section. Results obtained with experimental data are presented in the next section.

In the following simulations, we applied the implicit Euler scheme for the time discretization to avoid stability problems (the method is strongly A-stable as already mentioned above). However, a comparison with the second order Crank-Nicholson scheme showed no substantial differences with respect to the quality of the obtained heat flux estimations. The material properties chosen in this section do not reflect the real experimental data of Section 6 as we focus on method and code validation.

### 5.1 Example 1: Continuous and time varying heat flux

In Examples 1 and 2 we consider the domain  $\Omega := 10 \times 40 \times 100 \text{ mm}^3$ . The material properties for these cases are lumped in the parameter  $a = 10^{-4} \frac{\text{m}^2}{\text{s}}$ . For the time discretization (implicit Euler scheme) we use the time step size  $\tau = 0.01 \text{ s}$  and apply 200 time steps. The initial and known boundary conditions consist of a constant temperature distribution  $T(\mathbf{x}, t_0) = 20^\circ\text{C}$ ,  $\mathbf{x} \in \Omega$ , a constant heat flux  $q_h(\mathbf{x}, t) = 2 \frac{\text{kW}}{\text{m}^2}$ ,  $(\mathbf{x}, t) \in \Gamma_1 \times [t_0, t_f]$  for heat addition and perfectly isolated boundaries on  $\Gamma_r$  (cf. the notation of Section 2). For the start approximation within the optimization procedure, we choose  $q_c^0(\mathbf{x}, t) = 0 \frac{\text{kW}}{\text{m}^2}$ ,  $(\mathbf{x}, t) \in \Gamma_2 \times [t_0, t_f]$  (see Fig. 3).

In this first example a uniform space discretization with 35937 unknowns is applied (corresponding to an initial grid triangulation with  $32 \times 32 \times 32$  parallelepipeds and 196608 tetrahedra, for more details cf. [8]). As a basis of this simulation we choose a shape of the heat flux, which represents an intuitive approximation of the real quantity in the falling film experiment. This heat flux is denoted by  $q_c^{ex}(\mathbf{x}, t)$ ,  $(\mathbf{x}, t) \in \Gamma_2 \times [t_0, t_f]$  and has a sinusoidal pattern over the space coordinate in the flow direction of the falling film (i.e. the z-direction). The wavy pattern is assumed to be time dependent, such that the waves travel along the z-direction over time

$$q_c^{ex}(x, y, z; t) = \sin\left(4\pi\left(\frac{z}{100} + \frac{t}{200}\right)\right) \frac{\text{kW}}{\text{m}^2}, \quad (x, y, z) \in \Gamma_2, t \in [t_0, t_f].$$

### 5.1.1 Estimation with error-free measurements

First we present the estimation results of the boundary heat flux with error-free measurements. As measurement data we take the temperature  $T_m^{ex}$  obtained from the solution of the direct heat conduction problem with the chosen quantity  $q_c^{ex}$  as the corresponding boundary condition on  $\Gamma_2$ .

In Fig. 6 (a), the objective functional is plotted over the number of optimization iterations, whereas a snapshot (at one point in time) of the estimated heat flux at the end of the optimization is presented in Fig. 6 (b).

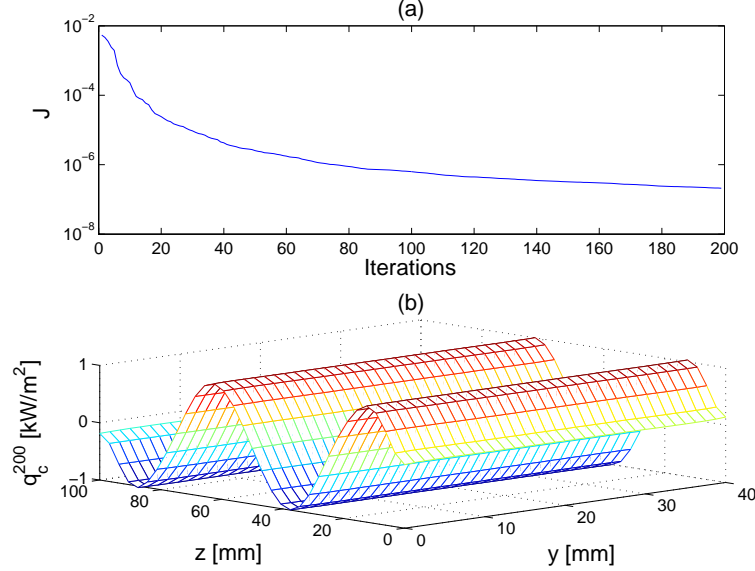


Fig. 6. (a) Objective functional (b) estimated heat flux  $q_c^{200}$

We observe the well known convergence behavior of the applied CG method in terms of a more rapid decrease of the objective functional at the beginning of the iterative process followed by stagnation at a certain level. Plot (b) shows that the estimated heat flux is, like the exact quantity, constant in  $y$ -direction. Therefore, we restrict the following plots to a cut through the  $y$ -axis to look at the estimation quality in more detail.

Both exact and estimated heat fluxes are given in Fig. 7 over the  $z$ -direction for constant  $y = 20 \text{ mm}$  (i.e. in the middle of the  $y$ -coordinate) and different numbers of time steps applied, which are denoted by  $ndt$ . Except for a region at final time the recovered heat flux is of high quality, since there are only little visible deviations compared to the exact quantity. At final time, the estimation quality decreases, due to the fact that the solution of the adjoint problem (i.e. the gradient of the objective functional) is zero and therefore causes no improvement of the start approximation for  $t = t_f$ . The effect of the iterative CG method is presented in Fig. 8. Here the error free and estimated heat fluxes are shown at the fixed time level  $ndt = 100$  and different iterations

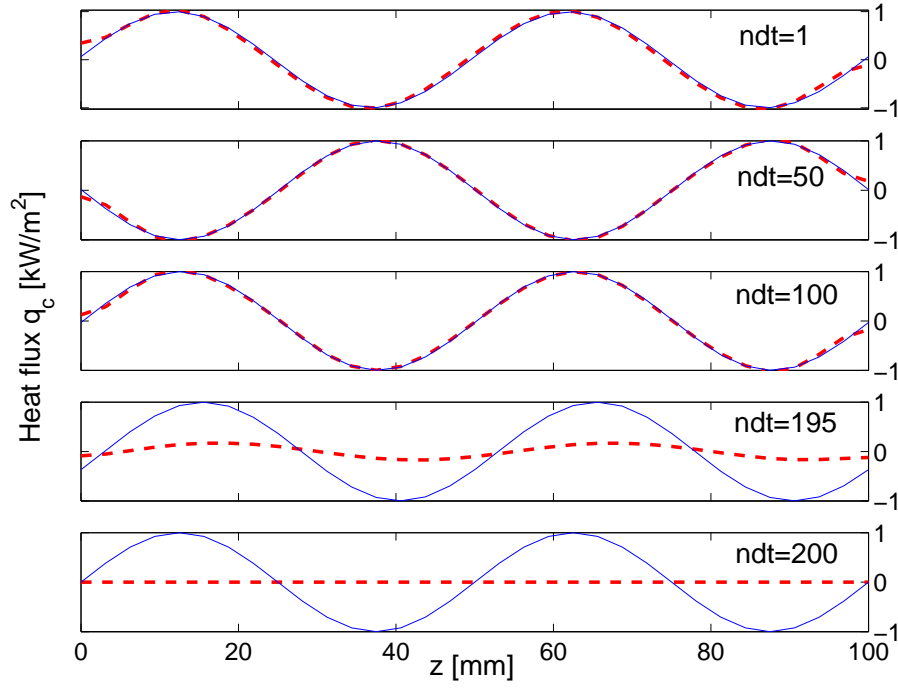


Fig. 7. Exact heat flux  $q_c^{ex}$  (solid line) and estimated heat flux  $q_c^{200}$  (dashed line) for different time steps  $ndt$

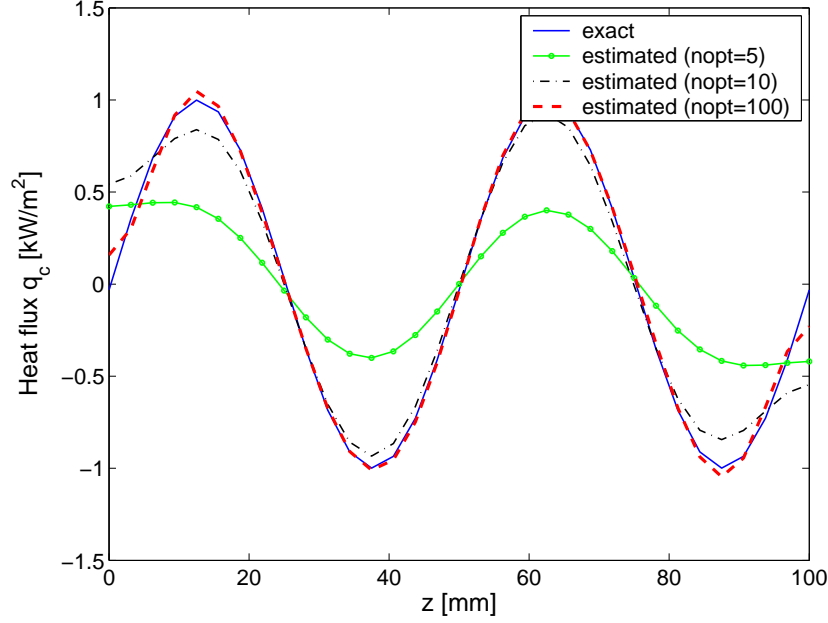


Fig. 8. Estimated heat flux for different optimization iterations  $nopt$

of the optimization, which are denoted by  $nopt$ . We clearly observe that the estimation quality increases with a rising number of optimization steps, since we use error-free temperature measurements. To stop the iterations, we consider the usual proceeding and specify a small threshold parameter  $\epsilon$  for the

objective function, i.e.

$$J(q_c^n) < \epsilon. \quad (25)$$

From Fig. 6 (a) we see that about 80 iterations are needed to satisfy the stopping rule (25) with  $\epsilon = 10^{-6}$ . Clearly, smaller values of  $\epsilon$  lead to more iterations.

### 5.1.2 Estimation in the presence of measurement errors

In this section, we perturb the exact temperature  $T_m^{ex}$ , obtained as described in the previous section, using an artificial measurement error  $\omega$ . We assume the perturbed temperature  $T_m$  given by

$$T_m = T_m^{ex} + \sigma\omega,$$

with  $\sigma$  being the standard deviation of the measurement error to be the corresponding measurement data. The values of  $\omega$  are generated from a zero mean normal distribution with variance one. The parameter  $\sigma$  is used to control the error amount added to the exact data. In the case of measurement errors, we cannot expect that the objective functional becomes arbitrarily small. To find an appropriate  $\epsilon$  to stop the iterations, we can use known parameter choice rules from the inverse problems literature [7].

The discrepancy principle suggests that we stop the iterations, when the residual approximately equals  $\sigma$ . From (5), we get the following expression for the threshold parameter  $\epsilon$  in (25)

$$\epsilon = \kappa(t_f - t_0)A_1\sigma,$$

where  $A_1$  is the surface of  $\Gamma_1$  and  $\kappa > 1$  is a parameter. In the following simulations we used  $\kappa = 1.02$ . A detailed discussion of this method is given in [7]. For  $\sigma = 0.25$  we obtain the optimal result after  $n_{opt} = 40$  iterations using the above considered stopping rule. The estimates and the corresponding temperatures are given in Fig. 9. A good reconstruction of the exact heat flux is achieved. By performing further iterations, the estimated heat flux begins to oscillate and the estimation quality decreases. Similar results have been obtained with higher values of the noise level  $\sigma$ .

An alternative stopping criterion is to use heuristic rules such as the L-curve [9], which is a parameterized plot of the residual against a solution norm. For  $\sigma = 0.25$ , the L-curve is shown in Fig. 10. The best compromise is found at the point of the L-curve with maximum curvature. For the considered case, the optimal value is about  $n_{opt} = 40$  iterations, i.e. the result is comparable to the one obtained by the discrepancy principle.

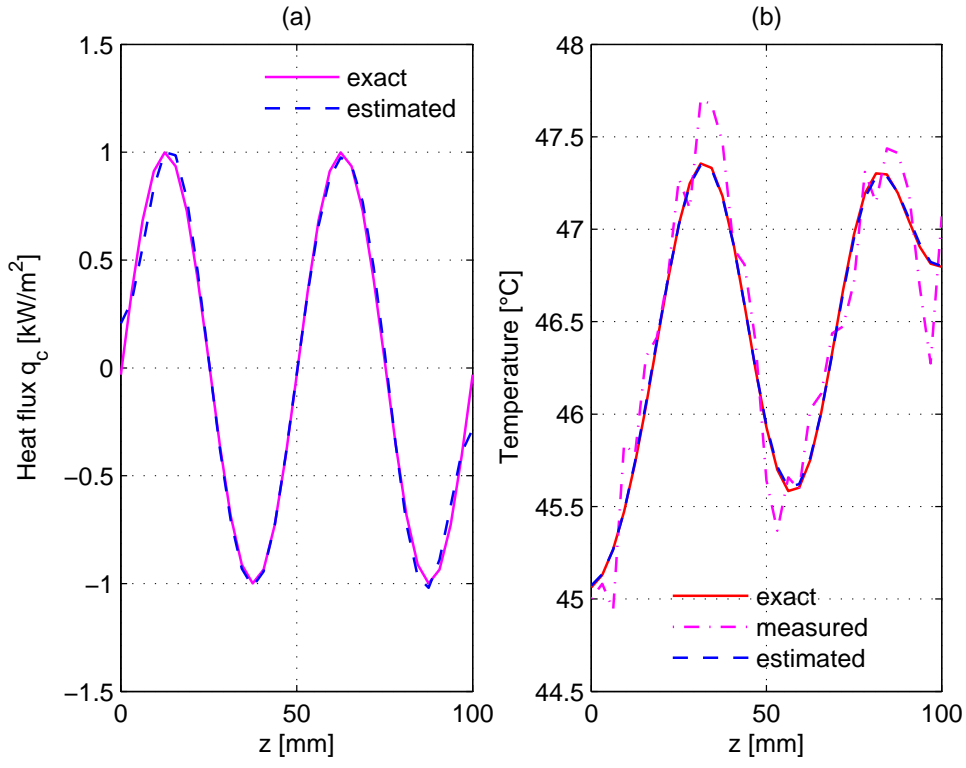


Fig. 9. Estimated heat flux with perturbed measurements  $\sigma = 0.25$  (a) exact and estimated heat flux  $q_c$  for  $nopt = 40$  (b) exact, measured and estimated temperature

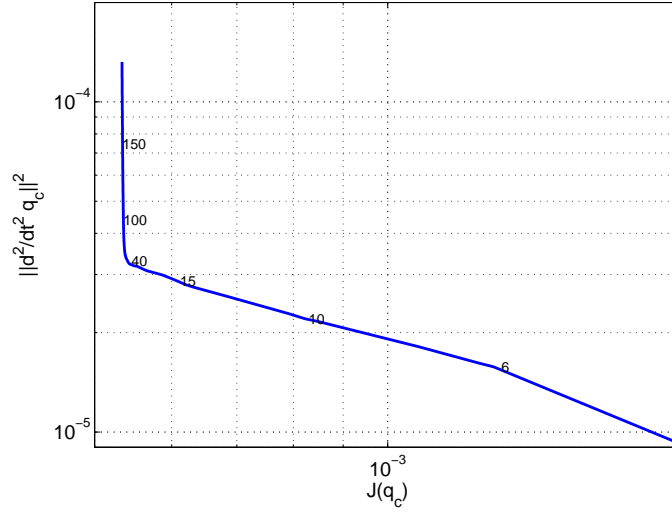


Fig. 10. L-curve for perturbed measurements with  $\sigma = 0.25$

## 5.2 Example 2: Discontinuous and steady state heat flux

In this section we present a simulation based on a heat flux  $q_c^{ex}$  that is time independent and discontinuous on  $\Gamma_2$ . Thus this heat flux does not belong to

the Sobolev space  $H^1(\Omega)$ . It has the representation

$$q_c^{ex}(x, y, z; t) = \begin{cases} 0 \frac{kW}{m^2} & \text{for } (x, y, z) \in \Gamma_0, \\ -3 \frac{kW}{m^2} & \text{else,} \end{cases}$$

with  $\Gamma_0 := \{(x, y, z) \in \Gamma_2 \mid y \in [10, 30] \vee z \in [20, 80]\}$  (see Fig. 11 (a)).

We again consider the situation described in the first paragraph of Example 1, but this time we use a quasi-uniform discretization with 36057 unknowns (corresponding to an initial triangulation with  $16 \times 20 \times 100$  parallelepipeds with respect to the space coordinates). We consider these data with focus on the real falling film experiment, where we choose a fine space discretization (resolution) in the flow direction ( $z$ -coordinate) and relatively coarse resolutions in the other directions (see Section 6).

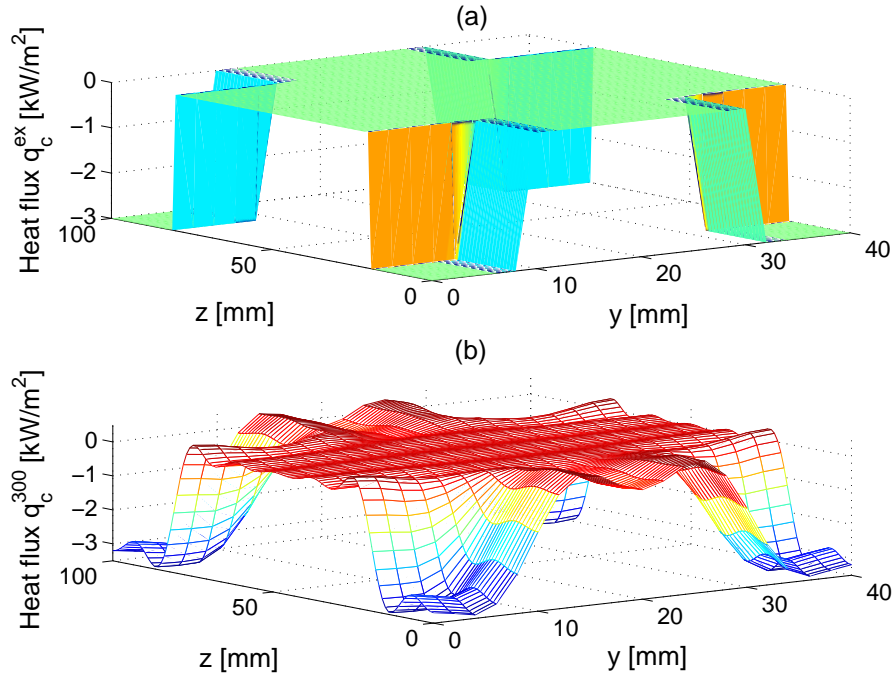


Fig. 11. Exact (a) and estimated (b) heat flux

The obtained estimation result is given in Fig. 11 (b). The objective functional shows the same typical behaviour as already described in Example 1 and therefore we do not give the plot here. Both, exact and estimated solutions of the inverse problem are given in Fig. 12 (a) and (b) for cuts through the  $y$ -axis and the  $z$ -axis respectively ( $y = 0$  and  $z = 0$ ). Again, results for different iteration numbers of the optimization procedure are shown.

Due to the discontinuities of the error free boundary heat flux, oscillations appear in the piecewise continuous approximations with an increasing number of optimization iterations applied. A comparison of both plots with 100 (a)



and 20 (b) unknowns in the corresponding space directions respectively shows a better approximation quality for the case with higher space resolution.

The number of unknowns needed to reach the desired accuracy should be kept as small as possible for efficiency reasons. Instead of refining the whole grid, it may be better to use locally refined grids. Local grid refinement leads to good approximation properties, while at the same time the number of unknowns is severely decreased compared to the global refinement case. The multilevel refinement algorithm, which is implemented in DROPS, makes it easy to use such locally refined triangulations. The solution of the considered IHCP on such grids remains a challenging task for future investigations. In this context, suitable error estimators have to be developed that are based on the spatial behaviour of the unknown quantity, which is not the solution of the direct problems (i.e. the temperature distributions) but the corresponding boundary condition on  $\Gamma_2$ .

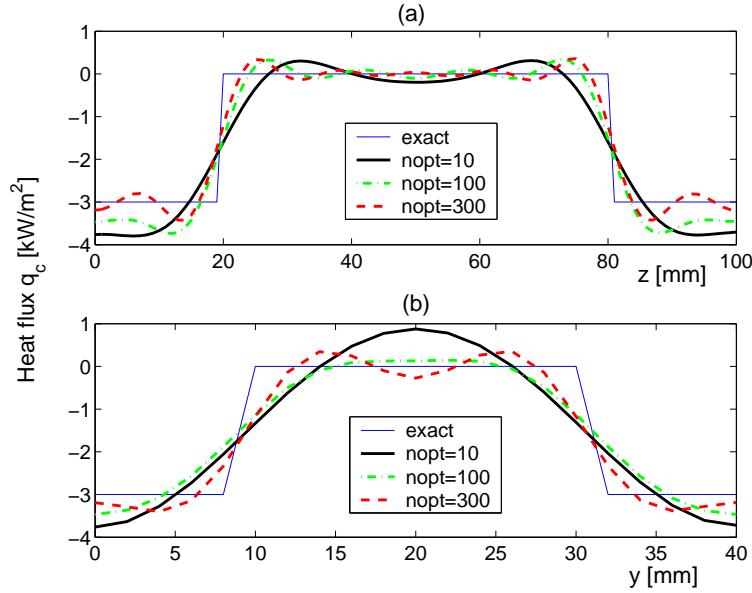


Fig. 12. 2D plots of the heat fluxes for  $y = 0$  (a) and  $z = 0$  (b) at different optimization steps  $n_{\text{opt}}$

The temperature distributions corresponding to the estimated quantities are shown in Fig. 13 (a) and (b) together with the exact values for different optimization steps. The plots show that we obtain high proximities to the exact temperature distributions after only few optimization iterations in contrast to the corresponding heat fluxes. This example shows, that the value of the functional is in general not a good measure for the quality of the estimation. The fit of the temperatures may be almost perfect, even though the estimated heat flux is quite different from the exact one. This largely unavoidable effect is due to the ill-posedness of inverse heat conduction problems caused by the strong smoothing properties of the direct problem.

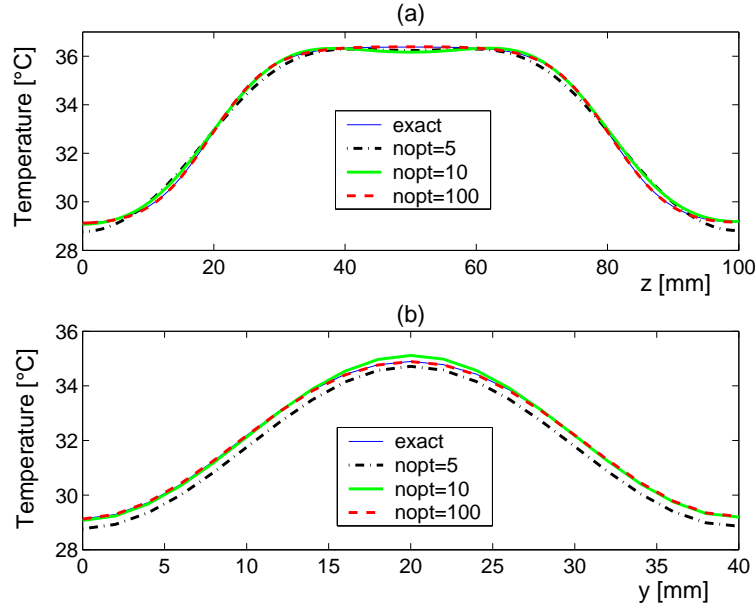


Fig. 13. 2D plots of the temperatures for  $y = 0$  (a) and  $z = 0$  (b) at different optimization steps  $n_{opt}$

## 6 Estimation results with measurement data

In this section, we present an estimation case study for the real falling film experiment employing high resolution temperature measurements. These are taken with an IR camera on the back side  $\Gamma_1$  of the constantan foil, which has a thickness of  $25 \mu m$ . The main idea behind choosing a very small heating foil consists in reaching a small temperature gradient across the foil thickness, i.e. the temperatures on both sides of the foil should be nearly identical. In that case, the measured data will be a good estimate of the temperature on the inaccessible film side of the foil. The measurement section has the dimension  $19.5 \times 39 \text{ mm}^2$ . Hence, we define the domain  $\Omega := 0.025 \times 19.5 \times 39 \text{ mm}^3$ . Due to this geometric anisotropy, we have to use degenerated finite elements (see Section 4).

The measurement data are taken with a sampling frequency of  $500 \text{ Hz}$  and a space resolution of  $100 \times 200 \text{ pixel}$ . These technical data translate to a time step size of  $\tau = 2 \text{ ms}$  in the one step  $\theta$ -scheme and a space discretization of  $100 \times 200$  unknowns in the  $y$ - $z$ -plane in the case of a one by one allocation, i.e. if we consider the same resolution for the measurement data and the numerical simulation. For the space discretization in the  $x$ -direction only 5 unknowns are used, which turns out to be an appropriate choice. To investigate the effect of the discretization on the temperature profile, we solved the direct problem for 5 and 9 unknowns in  $x$ -direction, respectively. As no additional frequencies appeared using the finer space mesh, we conclude that already the coarser grid is appropriate for the resolution of the temperature changes in that direction.

Altogether we get a space discretization with 472824 tetrahedra. The final time of the experiment is  $t_f = 0.3 \text{ s}$ , which corresponds to 150 temperature frames that are taken with the IR camera in order to observe the influence of some waves flowing off with the laminar falling film.

The electrical heating generates a constant heat flux  $q_h(\mathbf{x}, t) = 6.4 \frac{\text{kW}}{\text{m}^2}$ ,  $(\mathbf{x}, t) \in \Gamma_1 \times [t_0, t_f]$ . For the start approximation, we choose  $q_c^0(\mathbf{x}, t) = q_h$ ,  $(\mathbf{x}, t) \in \Gamma_2 \times [t_0, t_f]$ , because we expect  $q_c$  and  $q_h$  to have the same order of magnitude, due to the very thin heating foil. The other boundaries of the space domain are assumed to be perfectly isolated and the initial temperature distribution corresponds to the first temperature frame assumed to be constant across the foil thickness. The material properties of the foil are

$$\rho = 8900 \frac{\text{kg}}{\text{m}^3}, c = 410 \frac{\text{J}}{\text{kg K}}, \lambda = 23 \frac{\text{W}}{\text{m K}}.$$

resulting in a thermal diffusivity of  $a = 6.3 \cdot 10^{-6} \frac{\text{m}^2}{\text{s}}$ .

In Fig. 14 the measured temperature distribution over the y-z-plane at a certain point in time is shown. The plot clearly shows that these data are perturbed by a large amount of noise. Without going into more detail here, we mention the measurement preprocessing applied to the experimental data of the falling film. In order to remove the effect of the convective heat transport in the flow direction of the falling film, a reference picture is subtracted from all the temperature frames taken with the IR camera.

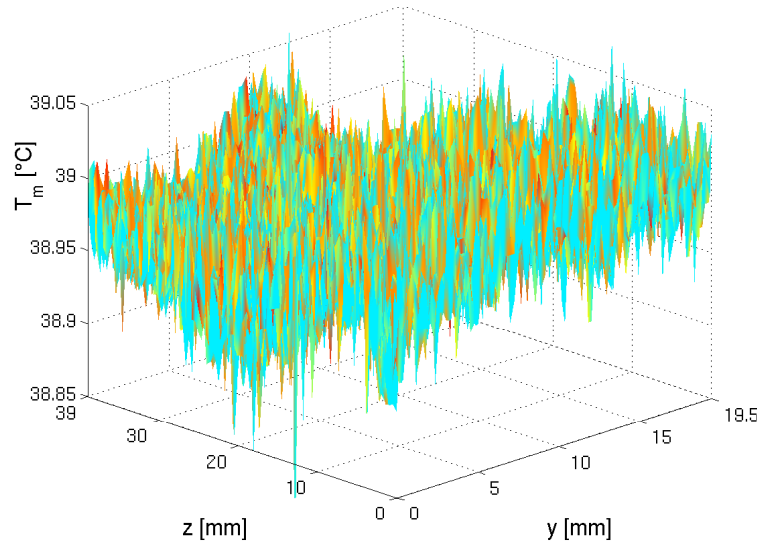


Fig. 14. Measured temperature data

A typical observation in the context of inverse problems deals with the effect of noise in the given input data with respect to the number of optimization iterations. Fig. 15 shows the evolution of the corresponding objective functional,

which decreases rapidly in the first iterations and flattens in the following steps. Although the temperature residual gets smaller, the quality of the corresponding estimated heat flux gets worse because of oscillations that appear with a rising number of optimization steps. This is an important reason why we have to investigate suitable regularization methods.

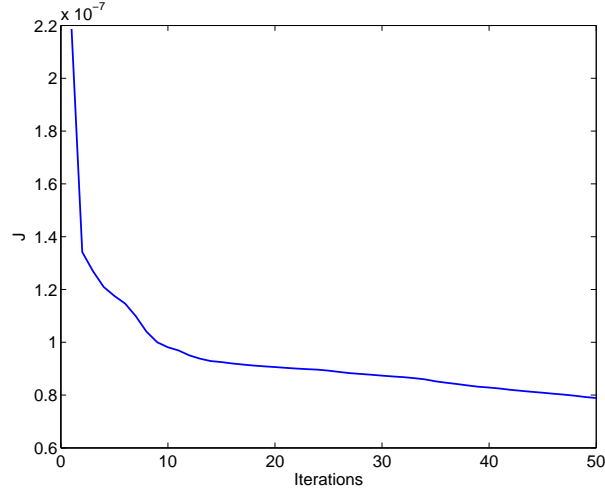


Fig. 15. Objective functional over iterations

In Fig. 16, the optimal solution computed on the basis of measured input data is presented over the given time interval. Here the estimated heat flux  $q_c^{15}$  is plotted for different time values. The discrepancy principle as described above has been used as a stopping rule resulting in  $n_{opt} = 15$  iterations. The estimated standard deviation of the measurement error is  $\sigma = 0.02$ . As a reference for the quality of the calculated result the measured temperature and the temperature determined by the computed heat flux are shown as well. The L-curve for this case is shown in Figure 17. We see that the optimal estimate is also obtained after 15 iterations, though the maximum curvature point is not very much exposed.

Looking at the solution over the time interval we observe that the estimated heat flux shows a wavy structure moving along in the flow direction of the falling film (i.e. the  $z$ -direction) with the same frequency as the film waves. This can be traced back to the influence of the wavy film surface whose varying thickness effects the amount of heat that is transferred from the foil to the film. The quality of the approximation decreases at the end of time, since the solution of the adjoint problem is zero at final time and therefore causes no improvement of the corresponding iterative solution.

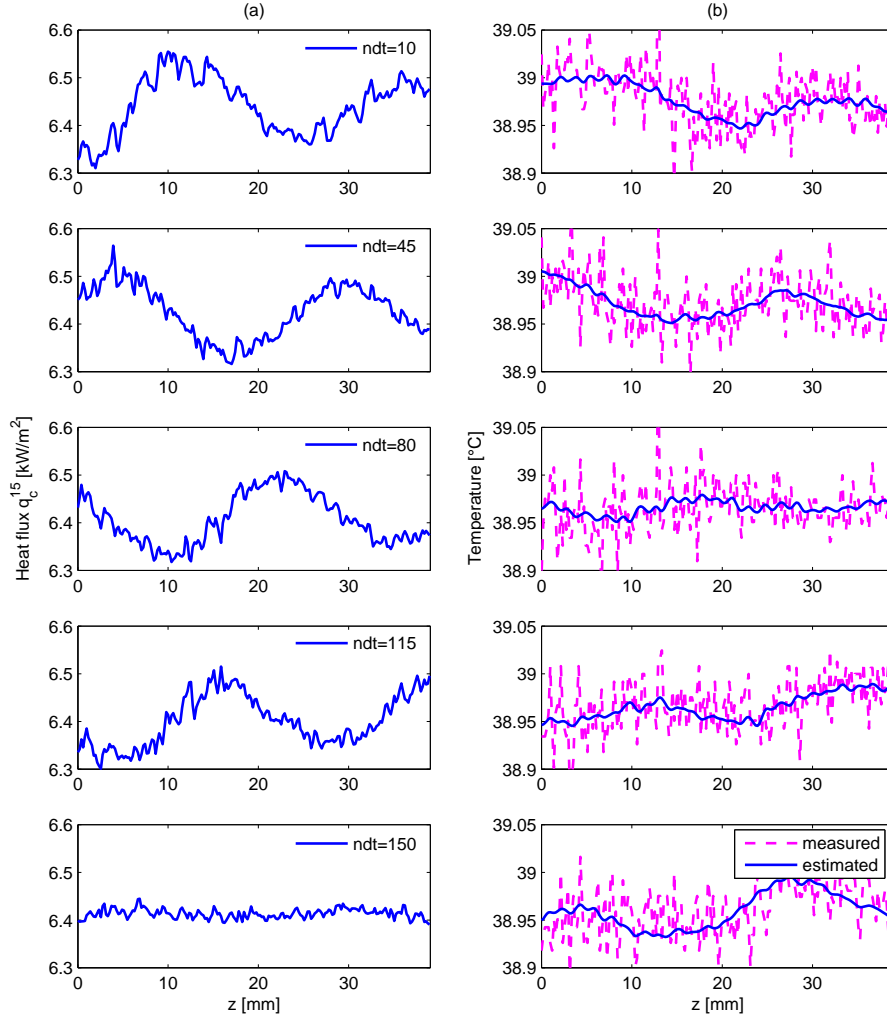


Fig. 16. Estimation result after 15 iterations at different time steps: Heat flux estimate  $q_c^{15}$  (a), measured (dashed line) and estimated temperature (solid line) (b)

## 7 Conclusions and future work

The conjugate gradient method has successfully been applied to the 3D transient inverse heat conduction problem in a falling film experiment to estimate the boundary heat flux at the film side of the heating foil from high resolution temperature measurements taken with an infrared camera at the foil back side. Simulation studies show that a time-dependent heat flux can be adequately predicted from the measurements within few iterations of the CG algorithm. The quality of the estimation depends on the level of the measurement error.

Future work will be devoted to the more complex problem of estimating the

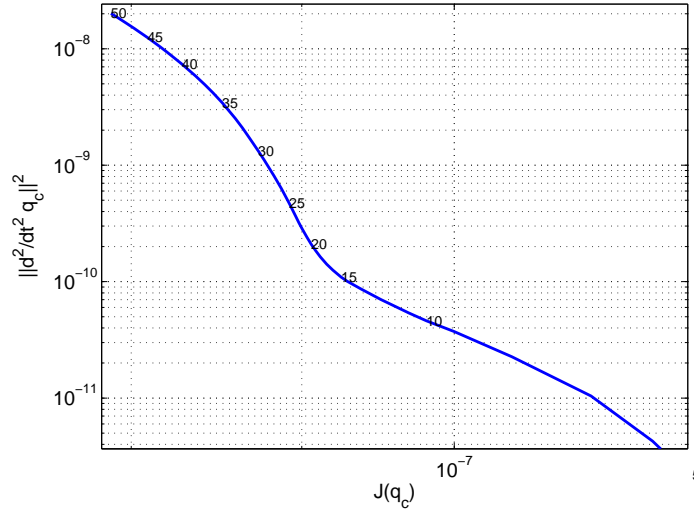


Fig. 17. L-curve for the measurement data

heat flux on the wavy surface of the falling film. For this task, we need to address momentum equations in addition to the energy equation including convective terms. The same algorithm can also be used for this case. Moreover, using the estimation procedure we can perform an optimal design of the experimental setup and determine conditions to enhance the information content of the measurements.

## Acknowledgements

Financial support from DFG (Deutsche Forschungsgemeinschaft) via the collaborative research center SFB 540 and the graduate program GRK 775 is gratefully acknowledged.

## References

- [1] F. Al-Sibai, A. Leefken, and U. Renz. Local and instantaneous distribution of heat transfer rates through wavy films. *International Journal of Thermal Sciences*, 41:658–663, 2002.
- [2] O. M. Alifanov. *Inverse Heat Transfer Problems*. Springer, Berlin, 1994.
- [3] U. M. Ascher and E. Haber. A multigrid method for distributed parameter estimation problems. *Electronic Transactions on Numerical Analysis*, 15:1–17, 2003.

- [4] I. Babuska and A.K. Aziz. On the angle condition in the finite element method. *SIAM J. Numer. Anal.*, 13:214–226, 1976.
- [5] J. V. Beck, B. Blackwell, and A. Haji-Sheikh. Comparison of some inverse heat conduction methods using experimental data. *International Journal of Heat and Mass Transfer*, 39(17):3649–3657, 1996.
- [6] S. Chantasiriwan. An algorithm for solving multidimensional inverse heat conduction problems. *International Journal of Heat and Mass Transfer*, 44:3823–3832, 2001.
- [7] H. W. Engl, M. Hanke, and A. Neubauer. *Regularization of Inverse Problems*. Kluwer Academic Publishers, Dordrecht, 1996.
- [8] S. Groß, J. Peters, V. Reichelt, and A. Reusken. The DROPS package for numerical simulations of incompressible flows using parallel adaptive multigrid techniques. Technical Report No. 211, IGPM, 2002. <http://www.igpm.rwth-aachen.de/reports/ps/IGPM211.ps.gz>.
- [9] C. Hansen. *Rank-Deficient and Discrete Ill-posed Problems: Numerical Aspects of Linear Inversion*. SIAM Monographs on Mathematical Modeling and Computation. SIAM, Philadelphia, U.S.A., 1998.
- [10] C.-H. Huang and S.-P. Wang. A three-dimensional inverse heat conduction problem in estimating surface heat flux by conjugate gradient method. *International Journal of Heat and Mass Transfer*, 42:3387–3403, 1999.
- [11] M. Krizek. On the maximum angle condition for linear tetrahedral elements. *SIAM J. Numer. Anal.*, 29:521–527, 1992.
- [12] A. Leefken, F. Al-Sibai, and U. Renz. Measurement of instantaneous heat transfer using a hot-foil infrared technique. In *Thermosense XXIII, Proceedings of SPIE, Orlando, USA, April 16-19, 2001*, volume 4630, pages 21–29, 2001.
- [13] T. Lüttich, A. Mhamdi, and W. Marquardt. Design, formulation and solution of multi-dimensional inverse heat conduction problems. *Accepted: Numerical Heat Transfer , Part B*, 2004.
- [14] W. Marquardt. Model-based experimental analysis: A systems approach to mechanistic modeling of kinetic phenomena. In R. Agrarwal C. A. Floudas, editor, *Proceedings of FOCCAPD*, pages 165–183, 2004.
- [15] K. W. Morton and D. F. Mayers. *Numerical Solution of Partial Differential Equations*. Cambridge University Press, Cambridge, New York, Melbourne, 1994.
- [16] J. Nocedal and S. J. Wright. *Numerical Optimization*. Springer, Berlin, Heidelberg, New York, 1999.
- [17] A. Quarteroni and A. Valli. *Numerical Approximation of Partial Differential Equations*. Springer, Berlin, Heidelberg, 1994.

- [18] Y. Saad. *Iterative Methods for Sparse Linear Systems, 2nd edition*. SIAM, Philadelphia, PA, 2003.
- [19] C. Yang and C. Chen. Inverse estimation of the boundary condition in three-dimensional heat conduction. *J. Phys. D. Appl. Phys.*, 30(15):2209–2216, 1997.